

Article

Speed Control for PMSM with Fast Variable-Speed Sliding Mode Control via High-Gain Disturbance Observer

Hengqiang Wang ^{1,2}, Guangming Zhang ^{1,*}  and Xiaojun Liu ¹

¹ School of Mechanical and Power Engineering, Nanjing Tech University, Nanjing 211816, China; wanghengqiang@njpi.edu.cn (H.W.); xiaojunliu@njtech.edu.cn (X.L.)

² School of Electrical and Control Engineering, Nanjing Polytechnic Institute, Nanjing 210048, China

* Correspondence: zgm@njtech.edu.cn

Abstract: Since robustness only exists on the sliding mode/surface, sliding mode control is non-globally stable. Therefore, shortening the time to reach the sliding mode is an important method of improving sliding mode robustness. However, there is an inherent contradiction between rapidity and overshoot. Therefore, ensuring rapid convergence without overshoot is a worthwhile research problem. Consequently, this paper proposes a design for a fast variable speed reaching law (FVSRL) to improve the quality of sliding mode control. The constructed approach rate is based on a variable speed term, an exponential term, and a fast term, ensuring rapid convergence without overshoot. At the same time, a high-gain disturbance observer is employed for feedforward compensation. Finally, the designed reaching law is validated by comparing it with conventional exponential approach rates and a new sliding mode reaching law, demonstrating its superior performance. Detailed comparative and quantitative analyses of the simulation results using the conventional exponential reaching law, the new sliding mode reaching law, and the FVSRL are performed, utilizing metrics such as integrated square error, integral time square error, integrated absolute error, and integral time absolute error.

Keywords: PMSM; sliding mode control; fast variable speed reaching law; high-gain disturbance observer

MSC: 93C10; 93C40; 93C73



Citation: Wang, H.; Zhang, G.; Liu, X. Speed Control for PMSM with Fast Variable-Speed Sliding Mode Control via High-Gain Disturbance Observer. *Mathematics* **2024**, *12*, 2036. <https://doi.org/10.3390/math12132036>

Academic Editor: Asier Ibeas

Received: 5 June 2024

Revised: 27 June 2024

Accepted: 28 June 2024

Published: 29 June 2024



Copyright: © 2024 by the authors. Licensee MDPI, Basel, Switzerland. This article is an open access article distributed under the terms and conditions of the Creative Commons Attribution (CC BY) license (<https://creativecommons.org/licenses/by/4.0/>).

1. Introduction

The benefits of the permanent-magnet synchronous motor (PMSM) include a simple structure and high power density in addition to high efficiency [1]. Therefore, the PMSM has been extensively used in high-precision CNC machine tools, robotics, aerospace, and other fields [2–4]. However, PMSMs are multi-variable systems characterized by strong coupling and are subject to various disturbances and uncertainties, including load disturbance, parameter mismatch, friction, and so on [5]. Therefore, the performances obtained by traditional linear control methods, such as the PI control strategy, are hardly satisfactory, due to applying directly a linear PI controller in a nonlinear system. Although compensation is inherently automatic in PI regulators for modeling error, compensation may not always work effectively, even for predictive control systems [6]. In recent decades, in order to overcome some of the problems arising from traditional PI controllers, many nonlinear control theories have been proposed and developed. These methods include fuzzy control [7], auto-disturbance rejection control [8], model predictive control [9], and sliding mode control (SMC) [10]. Recently, the concept of designing several kinds of nonlinear control law has become very popular, and the SMC strategy is one of the important examples. SMC is a kind of a variable-structure control strategy that changes the dynamics of the system through a switching control law. The method is insensitive to parameter variations and has fast dynamic response [3,11–13].

However, it should be noted that the sliding mode method has some deficiencies too. In the context of the future implementation of the switching control law, time delays may result in high-frequency, oscillatory behavior, referred to as chattering. SMC consists of two key components: the reaching law and the sliding mode surface. The reaching law is useful in controlling the system states on the sliding mode surface; however, the task of maintaining the system states precisely on the sliding surface with zero error is a never-ending problem, as discussed in [14]. Moreover, the system states wander across both sides of the sliding surface and, thus, incorporate chattering. Furthermore, the SMC is only robust in the sliding mode and does not lend the system global robustness. Therefore, elimination of chattering and remedial action for the absence of global robustness are two paramount areas in SMC. The choice of the reaching law is especially critical since it affects the manner by which the system states progress towards the sliding mode surface [15].

However, it has been established that the regular SMC cannot be brought to the equilibrium point in a finite time duration; thus, there is the terminal SMC that can steer the tracking error to the equilibrium point in a finite time duration [16]. As to the singularity problem of the terminal SMC performing for the PMSM system, another nonsingular terminal SMC has been developed [17]. In addition, some new types of reaching law have been developed. The conventional exponential reaching law (CERL) was initially proposed and designed by Academician Weibing Gao [18]. A novel sliding mode control method utilizing a new sliding mode reaching law (NSMRL) has been introduced. This approach effectively reduces inherent chattering and enhances the velocity of the system state in reaching the sliding mode surface [19]. A new switching-type reaching law for sliding mode control of discrete-time systems was proposed. The refined reaching law ensures faster convergence and better robustness of the controlled plant compared to the earlier approach, while also helping to satisfy the constraints of important signals in the system [20].

Since disturbance observers can accommodate external disturbances, this can enhance the control quality of the system, as indicated in the work of [21]. By incorporating a disturbance observer to estimate random incidental disturbances and then feeding forward these estimates into the SMC, superior control performance can be attained, due to reduced effects from higher control gain values [22]. As the extended-state observer is simpler in application and more robust, it has been established that the expected performance based on the estimation of interference is realized by applying the observer of interference with the application of the sliding mode technique indicated in other studies [23,24].

As enhancing PMSM control can improve motor performance, based on the above research, this paper proposes a composite control strategy by introducing high-gain disturbance observer (HGDO) and fast variable-speed sliding mode control (FVSSMC) algorithms to achieve better speed control performance for PMSM systems. Additionally, a new fast variable speed reaching law (FVSRL) is incorporated into FVSSMC, to shorten the settling time. While ensuring convergence time without overshoot, robustness is greatly improved. The main contributions of this paper can be summarized as follows:

- An FVSRL was built to handle the contradiction between responding quickly and over-shooting, as far as embedded system certification is concerned.
- There was coordination between the HGDO and the FVSSMC, which aimed at doing 78 feedforward compensation.
- From the aspect of anti-interference, when applying the fast variable reaching law, the FVSSMC had good anti-interference ability.
- This was done through comparing with other similar models—namely, CERL and NSMRL—in order to substantiate the ease of use and accuracy of the FVSRL. Detailed comparative and quantitative analyses of the simulation results were conducted, using integrated square error (ISE), integral time square error (ITSE), integrated absolute error (IAE), and integral time absolute error (ITAE).

The remaining sections of this study are structured as follows: Section 2 presents the mathematical model for the three-phase PMSM. Section 3 provides an overview of

how the HGDO gets involved in determining the unknown lumped disturbance and feeds back the estimated value to the FVSSMC. Section 4 covers the design of the controller, while Section 5 provides a simulation study to validate the proposed approaches. Our conclusions are presented in Section 6.

2. PMSM Modeling

Under the conditions of ignoring motor parameter variations and external disturbances, the mathematical model of a PMSM can be described by the following voltage equations [25]:

$$\begin{cases} u_d = Ri_d + L_d \frac{di_d}{dt} - p\omega_m L_q i_q \\ u_q = Ri_q + L_q \frac{di_q}{dt} + p\omega_m L_d i_d + p\omega_m \psi_f \end{cases}, \quad (1)$$

where the symbols represent the following:

- u_d and u_q are the d -axis and q -axis voltages, respectively.
- R is the stator resistance.
- i_d and i_q are the d -axis and q -axis currents, respectively.
- L_d and L_q are the d -axis and q -axis inductances, respectively.
- p is the number of pole pairs.
- ω_m is the mechanical angular velocity of the motor.
- ψ_f is the flux linkage of the permanent magnet.

For a surface-mounted PMSM where $L_d = L_q = L_s$ the torque equation T_e can be expressed as follows:

$$T_e = \frac{3}{2} p \psi_f i_q. \quad (2)$$

The motion equations of the PMSM [25] are given by

$$\frac{d\omega_m}{dt} = \frac{3p\psi_f}{2J} i_q - \frac{T_L}{J} - \frac{B}{J} \omega_m, \quad (3)$$

where B represents the viscous friction coefficient, J denotes the moment of inertia, and T_L stands for the load torque.

Variations exist of Equation (3), and (4) can be obtained as follows:

$$\begin{aligned} \frac{d\omega_m}{dt} &= -\left(\frac{B}{J} + \Delta a\right)\omega_m - \left(\frac{T_L}{J} + \Delta c\right) + \left(\frac{3p\psi_f}{2J} i_q - \Delta b\right) i_q \\ &= a\omega_m + bu - d, \end{aligned} \quad (4)$$

where $a = -B/J$, $b = 3p\psi_f/2J$, and $u = i_q$ represent the control laws to be designed; Δa , Δb , Δc denote the variations in the motor parameters, and d represents the disturbance caused by parameter and load changes as follows:

$$d = \Delta a\omega_m + \Delta bu + \Delta c + \frac{T_L}{J}. \quad (5)$$

3. Disturbance Estimation with High-Gain Disturbance Observer

3.1. Design of High-Gain Disturbance Observer

As shown by Equation (4), the disturbance term d , which is part of the PMSM system, has a significant impact on system performance, since d will appear in the control input directly. To improve the robustness of the system, it is essential to compensate for these disturbances. However, in practical applications, disturbance values are not directly measurable. This necessitates the development of a disturbance observer to obtain

disturbance information. Consequently, this paper proposes the design of an HGDO for disturbance estimation.

Serving as a high-gain disturbance observer, it incorporates the disturbance into a new system state to be estimated. By setting up high-gain feedback for error compensation, the observer’s dynamics are designed to be significantly faster than those of the system, thereby ensuring accurate state tracking.

To establish the system’s state equation, let the state variable $x_1 = \omega_m$ and the output $y = \omega_m$. From Equation (4), Equation (6) can be obtained as follows:

$$\begin{cases} \dot{x}_1 = ax_1 - d + bu \\ y = x_1 \end{cases} \quad (6)$$

We introduce the disturbance term $-d$ as a new state variable x_2 . In practical PMSM systems, the disturbance d changes slowly, allowing us to approximate its first-order derivative as zero. Consequently, the state-space equation of the system is formulated as follows:

$$\begin{cases} \dot{x}_1 = ax_1 + x_2 + bu \\ \dot{x}_2 = 0 \\ y = x_1 \end{cases} \quad (7)$$

By using x_1 and x_2 as the observed variables, we establish a high-gain feedback for the speed estimation error e . The extended disturbance observer is designed as follows:

$$\begin{cases} e = y - \hat{x}_1 \\ \dot{\hat{x}}_1 = a\hat{x}_1 + \hat{x}_2 + bu + \frac{\alpha_1}{\eta}e \\ \dot{\hat{x}}_2 = \frac{\alpha_2}{\eta^2}e \end{cases} \quad (8)$$

where $\eta > 0$, α_1 , and α_2 are positive real numbers, typically chosen to be very small, to ensure high gain. Using this HGDO, we can achieve $\hat{x}_1 \rightarrow x_1$ and $\hat{x}_2 \rightarrow x_2$.

3.2. Observer Stability Analysis

To demonstrate that the observer converges within a finite time, we derive the error state equation of the observer and analyze its stability using the Lyapunov stability theory.

Theorem 1. *According to the Lyapunov stability theory, the observer can be stabilized when the convergence condition of the observer can be obtained as*

$$\|\zeta\| \leq \frac{2\epsilon L \|PB\|}{\lambda_{\min}(Q)} \quad (9)$$

Proof of Theorem 1. We define the error state variables of the observer as ζ :

$$\zeta = [\zeta_1 \quad \zeta_2]^T \quad (10)$$

where $\zeta_1 = \frac{x_1 - \hat{x}_1}{\epsilon}$, $\zeta_2 = -d - \hat{x}_2$. Due to

$$\begin{aligned} \epsilon \dot{\zeta}_1 &= \epsilon \frac{\dot{x}_1 - \dot{\hat{x}}_1}{\epsilon} = \dot{x}_1 - \dot{\hat{x}}_1 \\ &= (ax_1 + bu - d) - \left(a\hat{x}_1 + \hat{x}_2 + bu + \frac{\alpha_1}{\epsilon}e \right), \\ &= (\epsilon a - \alpha_1)\zeta_1 + \zeta_2 \\ &= -\alpha'_1 \zeta_1 + \zeta_2 \end{aligned} \quad (11)$$

$$\begin{aligned}
 \varepsilon \dot{\zeta}_2 &= \varepsilon(-\dot{d} - \dot{x}_2) \\
 &= \varepsilon\left(-\dot{d} - \frac{\alpha_2}{\varepsilon^2}(x_1 - \hat{x}_1)\right) \\
 &= -\varepsilon \dot{d} - \frac{\alpha_2}{\varepsilon}(x_1 - \hat{x}_1) \\
 &= -\alpha_2 \zeta_1 - \varepsilon \dot{d}
 \end{aligned}
 \tag{12}$$

Therefore, the error state equation of the extended observer can be written as

$$\varepsilon \dot{\zeta} = A\zeta + \varepsilon B(-\dot{d}),
 \tag{13}$$

where $A = \begin{bmatrix} -\alpha_1 & 1 \\ -\alpha_2 & 0 \end{bmatrix}$, $B = \begin{bmatrix} 0 \\ 1 \end{bmatrix}$. The characteristic equation of the matrix A is given by

$$|\lambda I - A| = \lambda^2 + \lambda\alpha'_1 + \alpha_2 = 0,
 \tag{14}$$

where I represents the identity matrix, λ denotes the eigenvalue of A , and A can be made Hurwitz by appropriately choosing α'_1 and α_2 . Then, for any symmetric positive-definite matrix Q , there exists a symmetric positive-definite matrix P satisfying

$$A^T P + PA + Q = 0.
 \tag{15}$$

We define the Lyapunov function for the observer as

$$V = \varepsilon \zeta^T P \zeta.
 \tag{16}$$

Taking the derivative of V and combining it with Equation (15), the next equation is given by

$$\begin{aligned}
 \dot{V} &= \varepsilon \dot{\zeta}^T P \zeta + \varepsilon \zeta^T P \dot{\zeta} \\
 &= (A\zeta + \varepsilon B(-\dot{d}))^T P \zeta + \zeta^T P (A\zeta + \varepsilon B(-\dot{d})) \\
 &= \zeta^T A^T P \zeta + \varepsilon (-B\dot{d})^T P \zeta + \zeta^T P \dot{A} \zeta + \varepsilon \zeta^T P B (-\dot{d}) \\
 &= \zeta^T (A^T P + PA) \zeta + 2\varepsilon \zeta^T P B (-\dot{d}) \\
 &= -\zeta^T Q \zeta + 2\varepsilon \zeta^T P B (-\dot{d}) \\
 &\leq -\zeta^T Q \zeta + 2\varepsilon \|PB\| \cdot \|\zeta\| \cdot |-\dot{d}|
 \end{aligned}
 \tag{17}$$

Assuming the boundedness of the disturbance derivative, i.e., $|-\dot{d}| \leq L$, combining with Equation (17), we have

$$\dot{V} \leq -\lambda_{\min}(Q)\|\zeta\|^2 + 2\varepsilon L\|PB\|\|\zeta\|.
 \tag{18}$$

Therefore, the observer can be stabilized when $\dot{V} \leq 0$. Consequently, the convergence condition of the observer can be obtained as Equation (9). Thus, Theorem 1 is proved completely. \square

Remark 1. From Equation (9), it can be seen that the convergence rate of ζ is inversely proportional to the parameter ε , i.e., the smaller ε is, the faster the convergence rate will be.

4. Controller Design

4.1. Design of Fast Terminal Variable Speed Reaching Law

Gao [18] proposed the concept of convergence rate and designed a widely used CERL, which is expressed as

$$\dot{\sigma} = -\mu \text{sgn}(\sigma) - q\sigma,
 \tag{19}$$

where σ is the sliding surface, μ is the approach rate, q is the approach coefficient, and μ and $q > 0$. The phase portrait of the TERL is shown in Figure 1a.

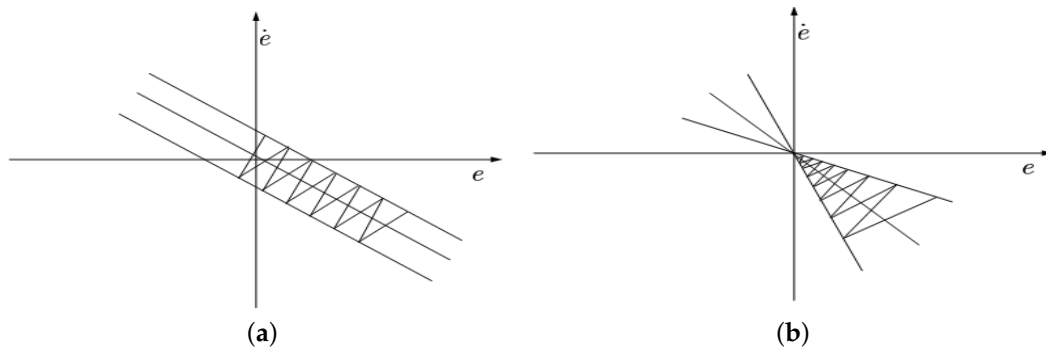


Figure 1. (a) CERL. (b) FSVRL.

As is well known, the conventional pure exponential reaching law cannot reach the sliding mode surface in finite time. To address this, an isokinetic reach term $\mu \operatorname{sgn}(\sigma)$ is added, ensuring that when σ is close to zero, the reaching velocity is μ instead of zero. However, while this addition resolves the accessibility problem, the reaching speed to the sliding mode surface in the exponential reaching law is determined by the design value of the parameter q . This creates a contradiction, as increasing the reaching speed simultaneously increases sliding chattering.

In order to solve the inherent chattering problem of the exponential reaching law, the above exponential reaching law was improved, to obtain a new type of fast variable speed reaching law (FVSRL), which is expressed as

$$\begin{cases} \frac{d\sigma}{dt} = -\mu|x|\operatorname{sgn}(\sigma) - k|\sigma|^\beta\operatorname{sgn}(\sigma) - q\sigma \\ \lim_{t \rightarrow \infty} |x| = 0, \mu > 0, q > 0, k > 0, 0 < \beta < 1 \end{cases} \quad (20)$$

where x is the error between the desired value and the real value. Due to the introduction of the variable term, the system can adaptively approach the sliding surface with exponential and variable speed rates and obtain a faster convergence speed. When the system state is far away from the sliding mode surface $-k|\sigma|^\beta\operatorname{sgn}(\sigma)$ and $-q\sigma$ play a major role. When the system approaches the sliding surface, the exponential terms $-k|\sigma|^\beta\operatorname{sgn}(\sigma)$ and $-q\sigma$ approach zero, and its effect becomes smaller. The speed term $-\mu|x|\operatorname{sgn}(\sigma)$ plays a major role. The system enters the sliding mode process and the selected state quantity x enters the sliding surface and moves toward the origin. At this time, the speed term $-\mu|x|\operatorname{sgn}(\sigma)$ also decreases as x decreases and, finally, stabilizes at the origin. When x decreases to zero, the speed term becomes zero, and the chattering is suppressed. The phase portrait of the FVSRL is shown in Figure 1b.

4.2. Sliding Mode Control Controller Design

Based on the HGDO and the FVSSMC, an entire PMSM control diagram is shown in Figure 2. The PMSM state variables via Equation (4) are given by

$$\begin{cases} x_1 = \omega_{cmd} - \omega_m \\ x_2 = \dot{x}_1 \end{cases} \quad (21)$$

The equation ω_{cmd} represents the target speed, while ω_m represents the motor output speed. Combining Equation (21) and taking the derivative of Equation (22) yields

$$\begin{cases} \dot{x}_1 = -(b i_q - a \omega_m + d) \\ \dot{x}_2 = -(b i_q - a \dot{\omega}_m + \dot{d}) \end{cases} \quad (22)$$

The definition of a sliding surface function is

$$\sigma = cx_1 + x_2. \tag{23}$$

The derivative of the sliding surface function is referred to as the “sliding mode control law”. Incorporating Equation (22) into this, we obtain

$$\dot{\sigma} = c\dot{x}_1 - bi_q + a\dot{\omega}_m - \dot{d}. \tag{24}$$

The integration of the HDGO and the SMC can be completed by using the observed value of d instead of d . This is also feedforward compensation. Combined with Equations (20) and (24) and substituting the observed disturbance and the perturbation value of the load torque \hat{d} into Equation (24) the output equation of the controller is obtained as

$$i_{q_{FVSSRL}} = \frac{1}{b} \int_0^t (c\dot{x}_1 + a\dot{\omega}_m + \mu|x|sgn(\sigma) + k|\sigma|^\beta sgn(\sigma) + q\sigma - \hat{d}) d\tau. \tag{25}$$

As seen from Equation (25), by incorporating parameter changes and load disturbances as feedforward compensation, the controller can counteract the effects of these disturbances on the system when the load and motor parameters vary.

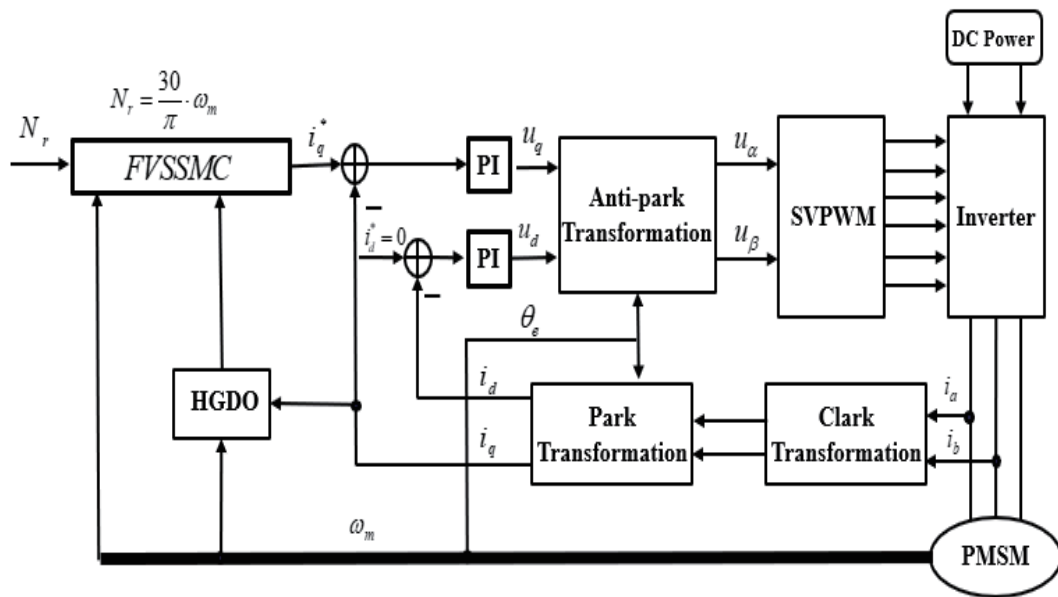


Figure 2. FVSSMC control chart based on HGO.

Based on the CERL and the NSMRL, the controllers used for comparison reference are as follows:

$$i_{q_{CERL}} = \frac{1}{b} \int_0^t (c\dot{x}_1 + a\dot{\omega}_m + \mu sgn(\sigma) + q\sigma - \hat{d}) d\tau, \tag{26}$$

$$i_{q_{NSMRL}} = \frac{1}{b} \int_0^t (c\dot{x}_1 + a\dot{\omega}_m + \lambda|x|^\rho sgn(s) - \chi|s|^\xi sgn(|s|^{-1})s - \hat{d}) d\tau. \tag{27}$$

Theorem 2. When the controller is chosen as in Equation (25), the stability of the motion system can be guaranteed.

Proof of Theorem 2. Select a Lyapunov function:

$$V = \frac{1}{2}\sigma^2. \tag{28}$$

According to the Lyapunov stability theorem, it is sufficient to prove that $\dot{V} < 0$ for the system to be asymptotically stable:

$$\begin{aligned} \dot{V} &= \sigma \dot{\sigma} \\ &= \sigma(c\dot{x}_1 - bi_q + a\dot{\omega}_m - \dot{d}) \end{aligned} \tag{29}$$

Substituting Equation (25) into Equation (29), Equation (30) is given by

$$\begin{aligned} \dot{V} &= \sigma \dot{\sigma} \\ &= \sigma \left(c\dot{x}_1 - b \left\{ \frac{1}{b} \left[c\dot{x}_1 + a\dot{\omega}_m + \mu|x|sgn(\sigma) + k|\sigma|^\beta sgn(\sigma) + q\sigma - \dot{d} \right] \right\} + a\dot{\omega}_m - \dot{d} \right) \\ &= -\sigma \left(\mu|x|sgn(\sigma) + k|\sigma|^\beta sgn(\sigma) + q\sigma \right) + \dot{d} - \dot{d} \\ &= -\mu|x||\sigma| - k|\sigma|^\beta|\sigma| - q\sigma^2 \leq 0 \end{aligned} \tag{30}$$

Therefore, Theorem 2 is proved completely. \square

5. Simulation

In this section, we present simulation results to demonstrate the effectiveness of the proposed control strategy. The simulation parameters of the model, observer, and controllers used in this study are summarized in Tables 1–3, respectively. Figure 3 shows a comparison of the times required for the CERL, NSMRL, and FTSVRL systems to achieve speed regulation, with the desired value set to 1000 rpm. As depicted in Figure 3, the FTSVRL achieved the desired speed of 1000 rpm in the shortest time of 0.1014 s, whereas the CERL and NSMRL required 0.335 s and 0.4366 s, respectively. Hence, this comparison indicates that the FTSVRL outperformed the CERL and the NSMRL. Figure 4 shows the corresponding current variations, which represent the changes in the control inputs. Moreover, Figure 5 presents detailed comparative and quantitative analyses of the simulation results for speed regulation, utilizing the ISE, ITSE, IAE, and ITAE metrics.

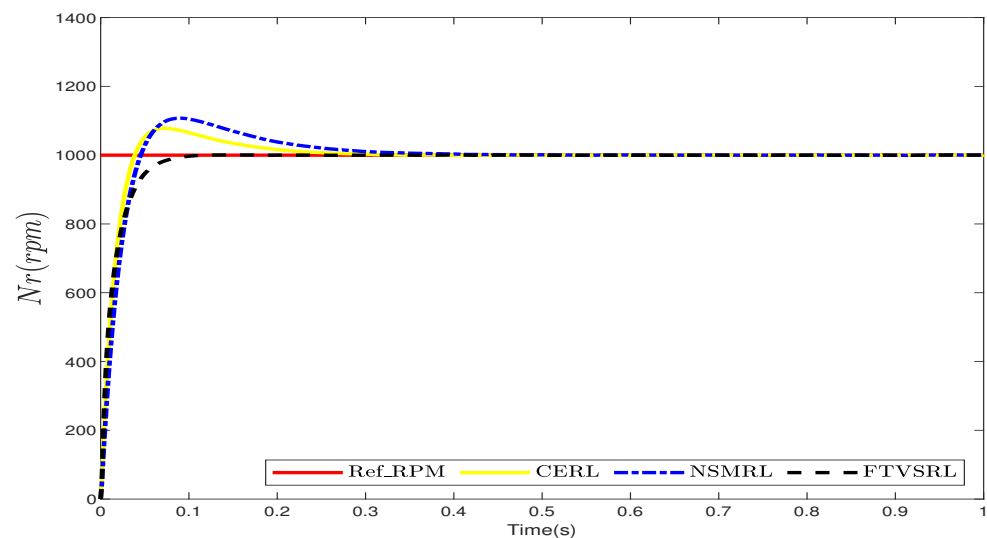


Figure 3. Comparison between CERL, NSMRL, and FTSVRL for speed regulation.

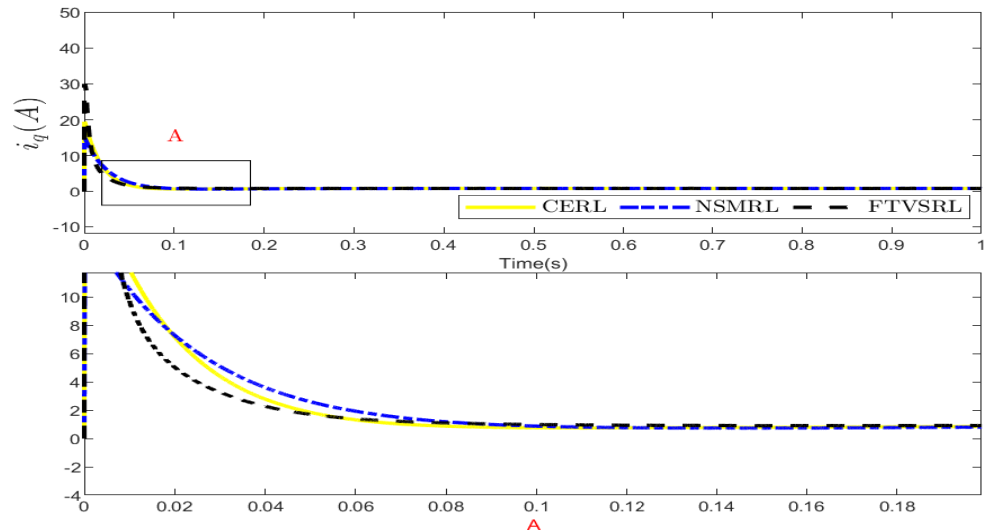


Figure 4. Comparison between CERL, NSMRL, and FTVSRL for control input of speed regulation.

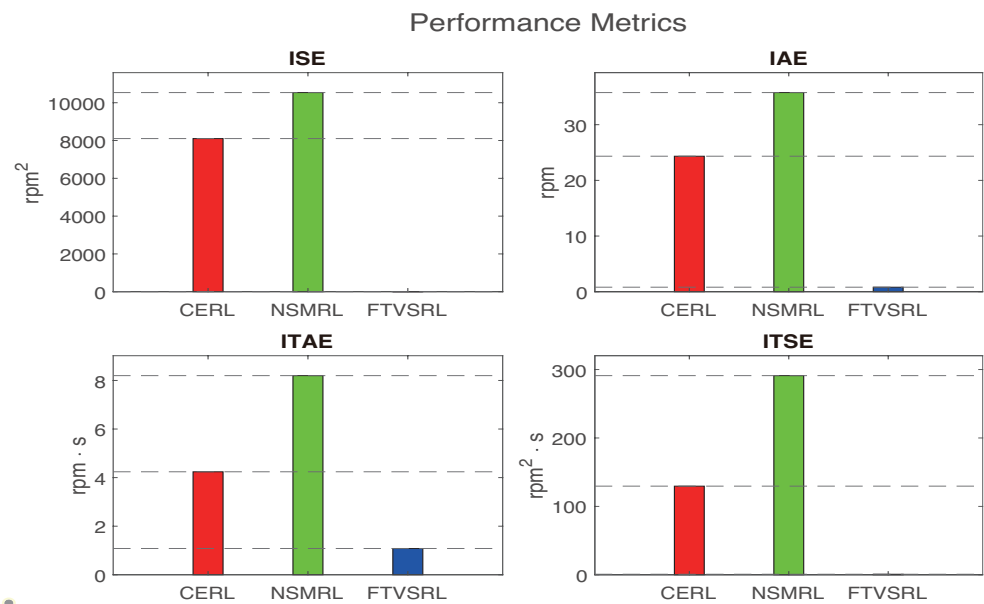


Figure 5. Performance index using ISE, IAE, ITAE, and ITSE for speed regulation.

To verify the efficiency of the developed control strategy, simulation experiments were performed for this section. Table 1 shows the different simulation parameters that were used in the current study, while Tables 2 and 3 depicts the different observers and controllers that were employed in the study, respectively. Figure 3 presents a comparison of the regulation times of the speed for the CERL, NSMRL, and FTVSRL systems, where the desired value was set to 1000 rpm. As seen in Figure 3, according to the requested performance, the FTVSRL rose to the required rotor speed of 1000 rpm within the shortest time of 0. The reaction times of the WSC, WEF, and Toll were 1014 s, whereas the CERL and the NSMRL required 0.335 s and 0.4366 s, respectively. Therefore, this comparison shows that the FTVSRL yielded better performance in comparison to the other two models, namely the CERL and the NSMRL. A similar but opposite result was obtained for the control inputs, as depicted in Figure 4, where the current differences are displayed. Furthermore, Figure 5 compares and quantifies the simulation results of the time–speed regulation, using the integrated square error (ISE), the integral time square error (ITSE), the integrated absolute error (IAE), and the integral time absolute error (ITAE).

Table 1. Parameter values of the PMSM.

| Parameters | Value | Unit |
|-------------------------|--------|---|
| Resistance R | 2.875 | $[\Omega]$ |
| Inductance L_s | 8.5 | $[\text{mH}]$ |
| Flux linkage ψ_f | 0.175 | $[\text{Wb}]$ |
| Inertia J | 0.0003 | $[\text{kg} \cdot \text{m}^2]$ |
| Damping coefficient B | 0.0008 | $[\text{N} \cdot \text{m} \cdot \text{s} / \text{r}]$ |
| Pole pairs p | 4 | |

Table 2. Parameter values of the HGDO.

| Parameters | Value |
|------------|--------|
| α_1 | 15 |
| α_2 | 9 |
| η | 0.0005 |

Table 3. Parameter values of the controllers.

| Controller | Value |
|------------|---|
| ERL | $\mu = 200, q = 50$ |
| NSMRL | $\lambda = 1, \chi = 30, \zeta = 0.01, \rho = 0.01$ |
| FVSRL | $\mu = 200, q = 50, k = 1050, \beta = 0.5$ |

Remark 2. For a fair comparison, all three controllers were equipped with the same HGDO and the same parameters. The relevant parameters are listed in Table 2.

Remark 3. To ensure the fairness of the comparison, c in Equation (23) was uniformly set to 15 for three comparisons. And the parameter values of the same parameters were set the same; the relevant parameters are listed in Table 3.

Figure 6 presents a comparison of the speed-tracking performances of the CERL, the NSMRL, and the FTSVRL. The desired speed changed from 0 to 900 rpm at 0.0901 s, then from 900 to -500 rpm at 0.4983 s, and from -500 to 500 rpm at 0.7488 s. These figures demonstrate that the FTSVRL outperformed the CERL and the NSMRL in terms of tracking performance. Figure 7 shows the corresponding changes in the current, which represents the control input. Additionally, Figure 8 provides detailed comparative and quantitative analyses of the simulation results for speed tracking, using the ISE, ITSE, IAE, and ITAE metrics.

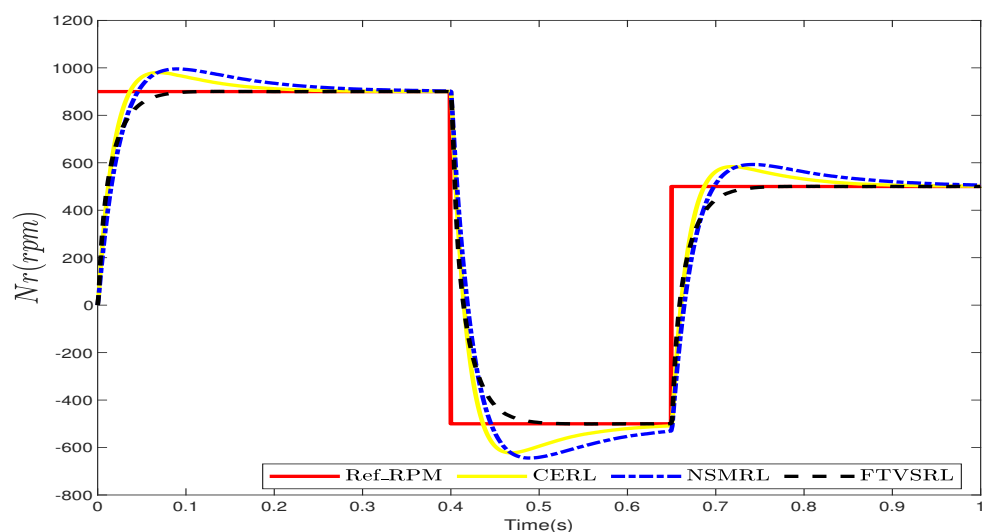


Figure 6. Comparison between CERL, NSMRL, and FTSVRL for speed tracking.

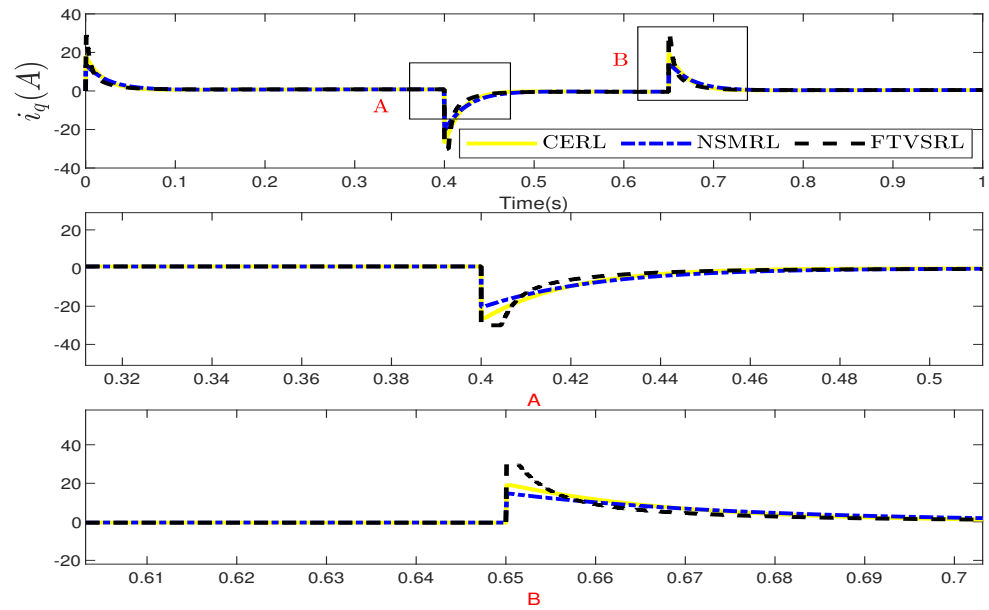


Figure 7. Comparison between CERL, NSMRL, and FTVSRL for control input of speed tracking.

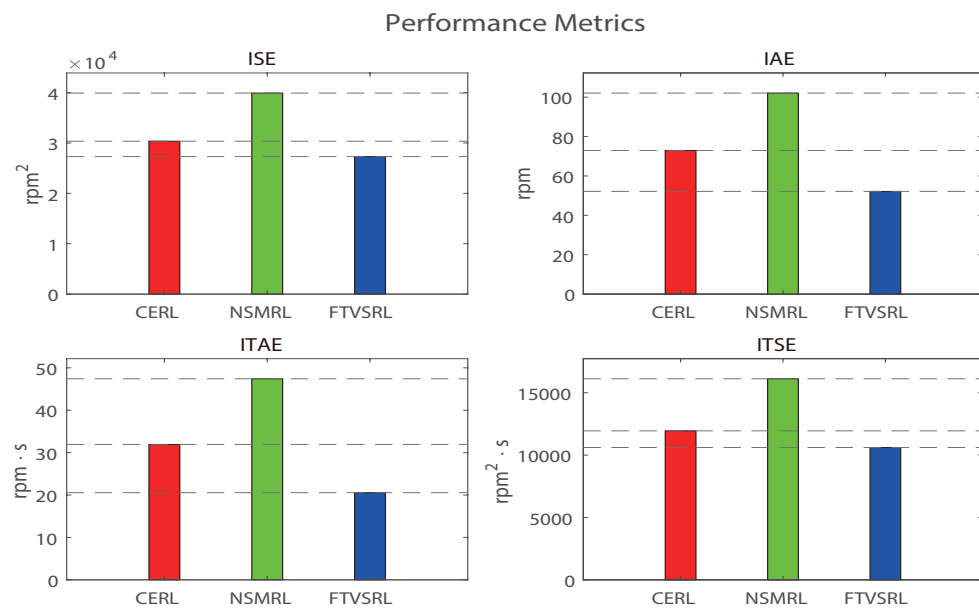


Figure 8. Performance index using ISE, IAE, ITAE, and ITSE for speed tracking.

Figure 9 shows the speed response of the motor to a sudden load of 10 N·m applied at 0.6 s. The load duration was 0.4 s, meaning the load was applied at 0.6 s and removed at 1 s. As shown in Figure 9, the FTVSRL achieved a smaller speed deviation from the desired speed than the CERL and the NSMRL, respectively. The corresponding changes in the current are shown in Figure 10. Furthermore, Figure 11 offers detailed comparative and quantitative analyses of the simulation results for the sudden load test, employing ISE, ITSE, IAE, and ITAE metrics.

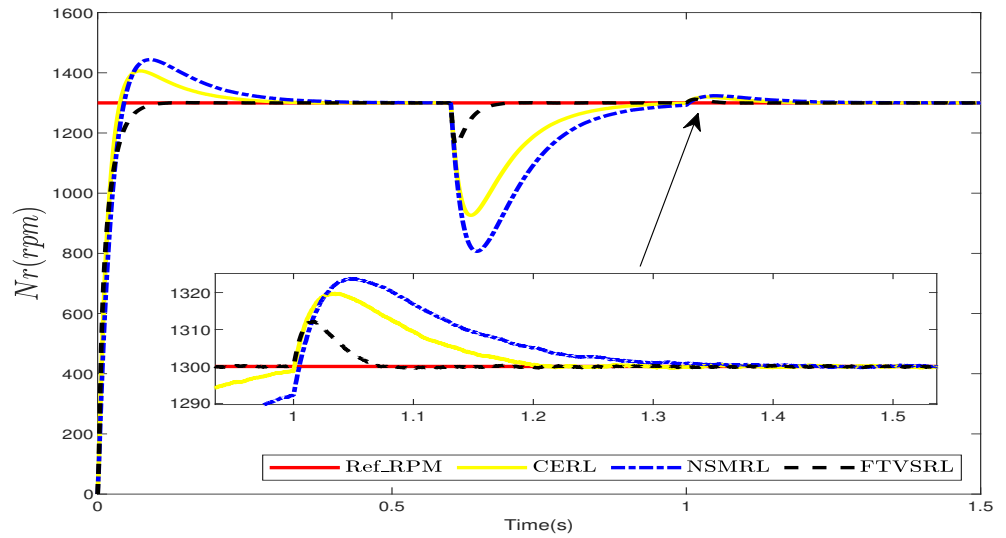


Figure 9. Comparison between CERL, NSMRL, and FTVSRL for sudden load test.

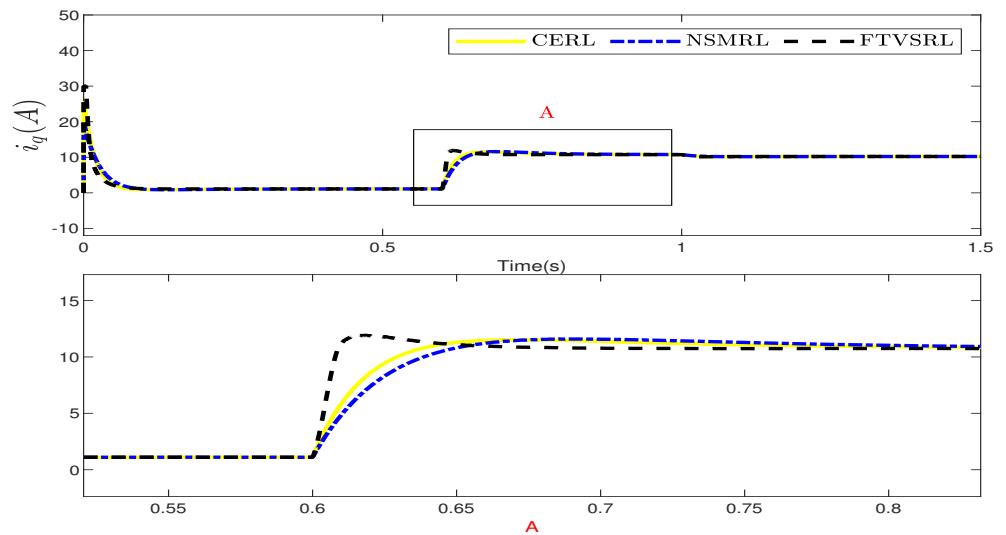


Figure 10. Comparison between CERL, NSMRL, and FTVSRL for control input of sudden load test.

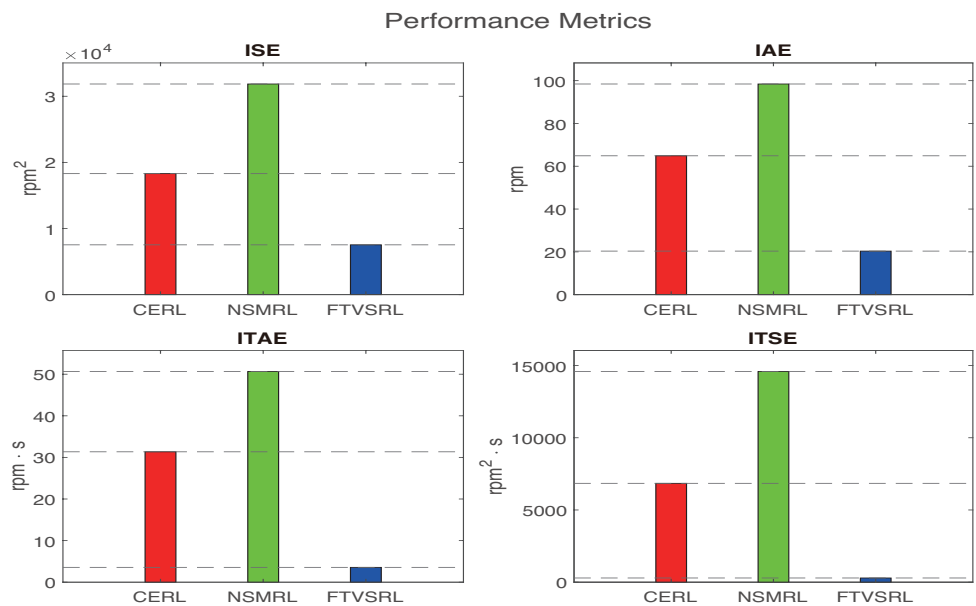


Figure 11. Performance index using ISE, IAE, ITAE, and ITSE for sudden load test.

6. Conclusions

To address the tension between rapid market responsiveness and ensuring comprehensive certification for embedded systems, the FVSRL was established. Collaborating with the HGDO alongside the FVSSMC, it enables feedforward compensation. Integrating the fast variable reaching law enriches the FVSSMC by mitigating interferences. Performance comparisons with other models, the CERL and the NSMRL, validated the usability and reliability of the FVSRL. These analyses utilized key performance parameters, including ISE, ITSE, IAE, and ITAE, for quantitative comparisons and simulations. In the future, we will use the designed reaching law to verify its performance on real motors.

Author Contributions: This paper was accomplished by all the authors. H.W. and G.Z. conceived the idea, performed the analysis, and designed the simulation; H.W. and X.L. carried out the numerical simulations; and H.W. wrote the manuscript. All authors have read and agreed to the published version of the manuscript.

Funding: This work was supported in part by the Science and Technology Innovation Project of the National Shuohuang Railway Company (SHTL-22-17) and in part by the Key Research Development Project of Nanjing Polytechnic Institute under Grant NJPI-2021-14.

Data Availability Statement: The original contributions presented in the study are included in the article material, further inquiries can be directed to the corresponding author.

Conflicts of Interest: The authors declare no conflicts of interest.

References

- Zhang, Z.; Yang, X.; Wang, W.; Chen, K.; Cheung, N.C.; Pan, J. Enhanced sliding mode control for PMSM speed drive systems using a novel adaptive sliding mode reaching law based on exponential function. *IEEE Trans. Ind. Electron.* **2024**. [[CrossRef](#)]
- Shi, T.; Wang, Z.; Xia, C. Speed measurement error suppression for PMSM control system using self-adaption Kalman observer. *IEEE Trans. Ind. Electron.* **2014**, *62*, 2753–2763. [[CrossRef](#)]
- Xu, W.; Junejo, A.K.; Liu, Y.; Islam, M.R. Improved continuous fast terminal sliding mode control with extended state observer for speed regulation of PMSM drive system. *IEEE Trans. Veh. Technol.* **2019**, *68*, 10465–10476. [[CrossRef](#)]
- Sun, X.; Cao, J.; Lei, G.; Guo, Y.; Zhu, J. A composite sliding mode control for SPMSM drives based on a new hybrid reaching law with disturbance compensation. *IEEE Trans. Transp. Electrification* **2021**, *7*, 1427–1436. [[CrossRef](#)]
- Sheng, L.; Li, W.; Wang, Y.; Fan, M.; Yang, X. Sensorless control of a shearer short-range cutting interior permanent magnet synchronous motor based on a new sliding mode observer. *IEEE Access* **2017**, *5*, 18439–18450. [[CrossRef](#)]
- Zhang, X.; Sun, L.; Zhao, K.; Sun, L. Nonlinear speed control for PMSM system using sliding-mode control and disturbance compensation techniques. *IEEE Trans. Power Electron.* **2012**, *28*, 1358–1365. [[CrossRef](#)]
- Kung, Y.S.; Tsai, M.H. FPGA-based speed control IC for PMSM drive with adaptive fuzzy control. *IEEE Trans. Power Electron.* **2007**, *22*, 2476–2486. [[CrossRef](#)]
- Liu, X.; Deng, Y.; Cao, H.; Wang, J.; Li, H.; Lee, C.H. Modified ADRC based on quasi-resonant fixed-time-convergent extended state observer for PMSM current regulation. *IEEE Trans. Transp. Electrification* **2024**. [[CrossRef](#)]
- Chen, Y.; Wang, X.; Xiao, D.; Ma, D.; Yang, X.; Wang, Z. Model predictive control of five-level open-end winding PMSM drives. *IEEE Trans. Transp. Electrification* **2024**. [[CrossRef](#)]
- Zwergger, T.; Mercorelli, P. Optimal control strategies for PMSM with a decoupling super twisting SMC and inductance estimation in the presence of saturation. *J. Frankl. Inst.* **2024**, *361*, 106934. [[CrossRef](#)]
- Sun, X.; Cao, J.; Lei, G.; Guo, Y.; Zhu, J. Speed sensorless control for permanent magnet synchronous motors based on finite position set. *IEEE Trans. Ind. Electron.* **2019**, *67*, 6089–6100. [[CrossRef](#)]
- Bai, C.; Yin, Z.; Zhang, Y.; Liu, J. Multiple-Models Adaptive Disturbance Observer-Based Predictive Control for Linear Permanent-Magnet Synchronous Motor Vector Drive. *IEEE Trans. Power Electron.* **2022**, *37*, 9596–9611. [[CrossRef](#)]
- Zheng, L.; Wu, C.; Shentu, F.; Wu, C. An Accurate Full-Speed Position Estimation for Permanent Magnet Synchronous Motors with a DC-Bus Current Sensor. *IEEE Trans. Power Electron.* **2024**. [[CrossRef](#)]
- Shtessel, Y.; Edwards, C.; Fridman, L.; Levant, A. *Sliding Mode Control and Observation*; Springer: Berlin/Heidelberg, Germany, 2014; Volume 10.
- Ma, H.; Wu, J.; Xiong, Z. A novel exponential reaching law of discrete-time sliding-mode control. *IEEE Trans. Ind. Electron.* **2017**, *64*, 3840–3850. [[CrossRef](#)]
- Ma, Y.; Li, D.; Li, Y.; Yang, L. A novel discrete compound integral terminal sliding mode control with disturbance compensation for PMSM speed system. *IEEE/ASME Trans. Mechatronics* **2021**, *27*, 549–560. [[CrossRef](#)]
- Yang, J.; Li, S.; Su, J.; Yu, X. Continuous nonsingular terminal sliding mode control for systems with mismatched disturbances. *Automatica* **2013**, *49*, 2287–2291. [[CrossRef](#)]

18. Gao, W.; Hung, J.C. Variable structure control of nonlinear systems: A new approach. *IEEE Trans. Ind. Electron.* **1993**, *40*, 45–55.
19. Hou, Q.; Ding, S. Finite-time extended state observer-based super-twisting sliding mode controller for PMSM drives with inertia identification. *IEEE Trans. Transp. Electr.* **2022**, *8*, 1918–1929. [[CrossRef](#)]
20. Bartoszewicz, A.; Leśniewski, P. New switching and nonswitching type reaching laws for SMC of discrete time systems. *IEEE Trans. Control Syst. Technol.* **2016**, *24*, 670–677. [[CrossRef](#)]
21. Ren, J.; Ye, Y.; Xu, G.; Zhao, Q.; Zhu, M. Uncertainty-and-disturbance-estimator-based current control scheme for PMSM drives with a simple parameter tuning algorithm. *IEEE Trans. Power Electron.* **2016**, *32*, 5712–5722. [[CrossRef](#)]
22. Hou, Q.; Ding, S.; Yu, X. Composite super-twisting sliding mode control design for PMSM speed regulation problem based on a novel disturbance observer. *IEEE Trans. Energy Convers.* **2020**, *36*, 2591–2599. [[CrossRef](#)]
23. Zhang, X.; Hou, B.; Mei, Y. Deadbeat predictive current control of permanent-magnet synchronous motors with stator current and disturbance observer. *IEEE Trans. Power Electron.* **2016**, *32*, 3818–3834. [[CrossRef](#)]
24. Wu, Y.j.; Li, G.f. Adaptive disturbance compensation finite control set optimal control for PMSM systems based on sliding mode extended state observer. *Mech. Syst. Signal Process.* **2018**, *98*, 402–414. [[CrossRef](#)]
25. Zhang, D.; Zhang, H.; Li, X.; Zhao, H.; Zhang, Y.; Wang, S.; Ahmad, T.; Liu, T.; Shuang, F.; Wu, T. A PMSM control system for electric vehicle using improved exponential reaching law and proportional resonance theory. *IEEE Trans. Veh. Technol.* **2023**, *72*, 8566–8578. [[CrossRef](#)]

Disclaimer/Publisher’s Note: The statements, opinions and data contained in all publications are solely those of the individual author(s) and contributor(s) and not of MDPI and/or the editor(s). MDPI and/or the editor(s) disclaim responsibility for any injury to people or property resulting from any ideas, methods, instructions or products referred to in the content.